ChemPubSoc
Europe

DOI: 10.1002/cctc.201402404

Spatial Concentration and Temperature Profiles in Dual-Packed-Bed Catalytic Reactors: Oxidative Coupling of Methane

Bahman Zohour, Daniel Noon, and Selim Senkan*[a]

Oxidative coupling of methane (OCM) is a complex surface catalysis and gas-phase reaction process to transform methane into ethane, ethylene and higher molecular weight hydrocarbons (C_{2+}). However, the C_{2+} product yields in single-pass fixed-bed reactors have been limited by the intrusion of gas-phase combustion reactions. To remedy this problem, a dual-bed OCM reactor configuration was explored in which the O_2 feed was distributed between two sequential packed bed reactors with interstage cooling using La_2O_3–CeO_2 nanofiber fabric catalysts. At the overall CH_4/O_2 feed ratio of 4.0, the dual-bed reactor configuration with split O_2 introduction resulted in the ultimate C_{2+} product yield of 21%, which is significantly higher than the 16% observed in the single-bed OCM reactor. In addition, spatially resolved species concentration and temperature profiles along the entire length of the dual-bed reactor were also acquired by using in situ microprobe sampling.

Oxidative coupling of methane (OCM) is a complex surface catalysis and gas-phase reaction process to convert natural gas into ethane and ethylene, which are valuable intermediates for the chemical industry.[1,2] In spite of decades-long research and many OCM catalysts reported,[2] no commercially viable catalyst has been developed. There appears to be an upper limit of C_{2+} yield of approximately 25% per reactor pass, which has been attributed to the intrusion of gas-phase combustion reactions at high temperatures.[3] Therefore, catalyst design alone may not be sufficient to result in the breakthrough needed for the commercialization of the OCM process. Consequently, a combined effort, both in catalyst development and in novel reactor systems and operating schemes are needed to advance the field.[4]

Early reactor simulations that used global OCM reaction kinetics were particularly encouraging, as they suggested the feasibility for attaining yields for C_{2+} products as high as +50% if the O_2 feed was distributed along the reactor, that is, by using membrane-type reactors.[5–7] Although these predictions may not be realistic, as the global reaction models used are well recognized to be of limited predictive value, they nevertheless create optimism regarding the future of the OCM process. More realistic and accurate predictions of the attainable yields can be accomplished by using detailed chemical kinetic mechanisms (DCKM). DCKM comprise a comprehensive description of chemical transformations in terms of irreducible chemical events or elementary reactions. DCKM, in conjunction with transport models, are crucial not only to correlate available experimental data but also to predict performance well outside the ranges of parameters investigated, including conditions under which the acquisition of the experimental data may be infeasible, for example, higher pressures and temperatures. However, the development and validation of DCKM require experimental data of high information content because of the presence of a large number of species participating in an even larger number of elementary reactions.

Recently, we reported spatial temperature and species concentration profiles in a packed-bed OCM reactor acquired by microprobe sampling.[8] This information-rich data, in addition to being particularly useful for DCKM work, revealed the early, that is, prompt, formation of H_2 in the OCM process, even before the formation of C_2H_6. This discovery suggested that the existing DCKM for the OCM processes[9,10] clearly must be revised to render them useful for predictive purposes. Our previous work[8] also demonstrated a significant weakness of using traditional integral reactor data, that is, reactor exit measurements, to develop reaction mechanisms.

Herein, we report for the first time spatially resolved species concentration and temperature profiles in a dual fixed-bed OCM reactor with interstage O_2 injection by using microprobe sampling[8] and demonstrate that the yields of C_{2+} products in the OCM can significantly be increased by distributed O_2 feed, as noted earlier.[5–7] The information-rich spatial profiles also provide new quantitative insight into the close coupling of the formation of C_{2+} products and O_2 levels in OCM reactors and, as such, should be valuable for the improvement and validation of predictive models.

Experimental Section

Experiments were performed by using a dual fixed-bed tubular reactor system, as shown in Figure 1. The reactor was sequentially packed with La_2O_3–CeO_2 nanofiber fabric catalysts that were prepared by electrospinning a viscous solution of polyvinylpyrrolidone (PVP, 0.60 g, 1.3 MDa), water/ethanol ($\approx$1:1 w/w, 9.5 g) into which the metal precursor (0.35 g), as $La(NO_3)_3{\cdot}6H_2O$ and $Ce(NO_3)_3{\cdot}6H_2O$, were dissolved having a La/Ce weight ratio of 3.[11] The electrospun material was calcined at 625 °C in a furnace to form metal-oxide nanofiber fabrics. SEM images confirmed that the nanofibers had an average diameter of approximately 90 nm. The fabric also had a low BET area of approximately 20 $m^2 g^{-1}$, which suggested that the nanofibers were dense and did not possess internal porosity.

[a] B. Zohour, D. Noon, Prof. Dr. S. Senkan
Department of Chemical and Biomolecular Engineering
University of California, Los Angeles CA 90095 (USA)
E-mail: ssenkan@gmail.com

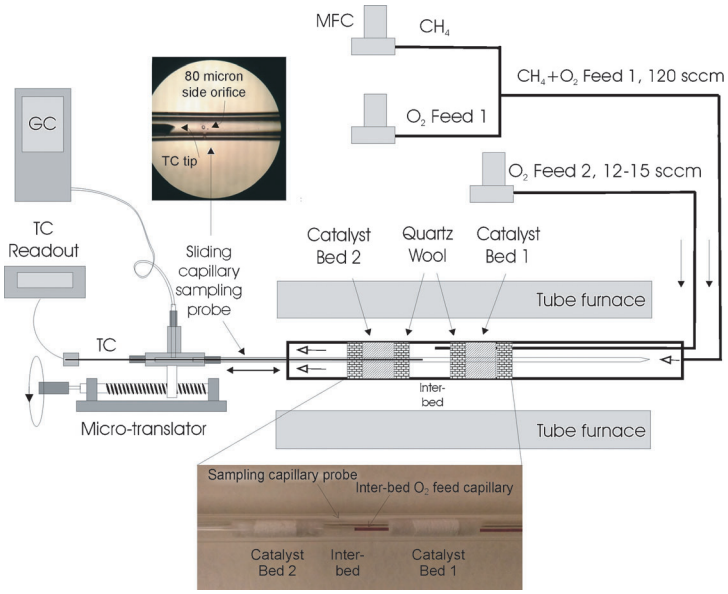

Figure 1. The reactor system used to acquire spatial temperature and concentration profiles. The reactor is a 6 mm diameter quartz tube packed with two 20 mg La_2O_3–CeO_2 nanofiber fabric catalyst beds (10 mm deep). Each bed is sandwiched between 20 mg quartz-wool plugs (5 mm deep), with an interbed spacing of 15 mm. The reactants are fed to the first reactor at a rate of 120 mL s^{-1} STP. A second O_2 feed is introduced to the middle of the interbed through a capillary tube at a rate of 12–15 mL s^{-1} STP. Gas samples were withdrawn from within the packed bed by using an 800 μm closed-end capillary tube with four approximately 80 μm side sampling orifices that was centrally inserted into the reactor bed. Gas analysis was accomplished by on-line gas chromatography. Spatial profiles were generated by sliding the capillary within the packed bed by using a microtranslation device. Temperature profiles were measured by a 250 μm diameter K-type thermocouple (TC) that was inserted into the capillary in separate experiments. The tip of the thermocouple was placed at the same location of the sampling orifice. Close-up images of the packed reactor (bottom) and the capillary sampling probe (top) are also shown.

As shown in Figure 2, two sections each with 20 mg of this fabric was loosely packed into a 6 mm diameter quartz tube (≈10 mm bed depth) and sandwiched between two 20 mg quartz wool plugs (≈5 mm bed depth). The interbed spacing was approximately 15 mm long. The bulk density and void fraction of the catalytic beds were determined to be approximately 0.3 g cm^{-3} and 0.94, respectively. The dual-bed reactor was placed inside a cylindrical tubular furnace to preheat the feed gases. In all experiments, the flow rate of the reactant gases to the first bed was maintained at 120 cm^3 min^{-1} at STP (mL min^{-1}) by using electronic mass flow controllers (MFC, MKS Billerica, MA). This flow rate corresponds to a nominal space time of approximately 60 ms per bed. The interstage O_2 was introduced at the middle of the interspace, that is, at approximately 27–28 mm by using a quartz capillary feed tube (800 μm, Friedrick and Dimock, Millville, NJ) at a rate of 12–15 mL min^{-1} (see Figure 2). The experiments were performed at 101.3 kPa.

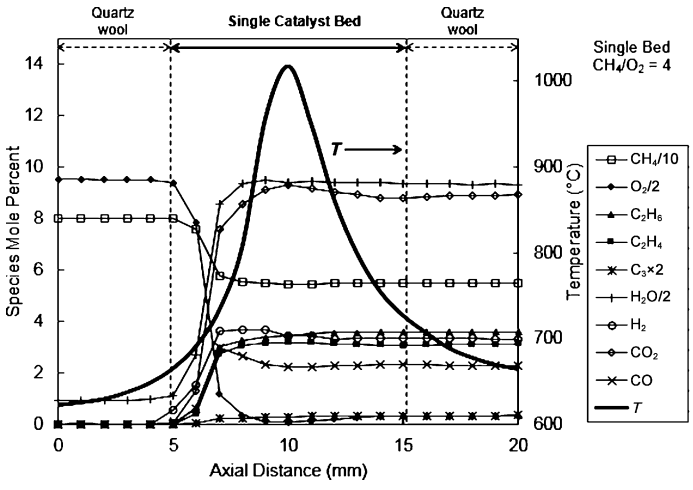

Figure 2. Spatial temperature and species mole percent profiles for a feed CH_4/O_2 ratio of 4. Total gas flow rate was 120 cm^3 min^{-1}, which corresponds to a nominal space time of approximately 70 ms (SB1).

Gas sampling was accomplished by centrally inserting a conically tapered and closed end quartz capillary tube into the packed beds followed by gas analysis by on-line gas chromatography (Varian 4900 Mini GC, with molecular sieve 5A and Poraplot U columns). The sampling capillary had four perpendicularly oriented 80 μm diameter orifices laser drilled on its side[12,13] to withdraw gases from within the bed (see inset in Figure 1). The location of the sampling orifice and the overall length of the probe were designed such that the capillary tip remained well outside both packed beds at any sampling position to avoid gas bypass within the beds. The sampling capillary probe withdrew gases at a rate less than 5 mL min^{-1}, which thus minimally perturbed the flow within the reactor (total flow ≈120–135 mL min^{-1}). This sampling rate corresponded to an average gas velocity of 50–100 cm s^{-1} within the capillary (depending on the temperature), which enabled the rapid removal of the gas samples from within the reactor. The fact that the measured concentration profiles remained flat, that is, did not change with axial position within the quartz wool, the interstage section, and reactor exits further supports the notion that reactions inside the sampling capillary were unimportant in our experiments. Temperature measurements were performed by placing a thin (250 μm diameter) K-type thermocouple inside the sampling capillary probe in the absence of gas withdrawal. The tip of the thermocouple was positioned at the sampling orifice. The possible presence of radial-temperature gradients was also explored by simultaneously placing multiple thermocouples at the same axial position but at different radial positions during the reaction. These measurements indicated maximum radial temperature differences in the 10–20 °C range at peak reactor temperatures of 800–1000 °C. Consequently, treatment of the reactor as quasi 1 D appears to be a reasonable assumption.[8] Capillary sampling lines outside the reaction furnace as well as GC injection system were heated to approximately 100 °C to prevent water condensation in the transfer lines. Water subsequently was condensed out by using an ice bath before GC analysis. Temperature and concentration profiles were obtained by moving the capillary (with and without the thermocouple) in the axial direction by using a micropositioning device (Velmex, Bloomfield, NY). Positional accuracy associated with the placement of the capillary probe within the reactor was estimated to be ±0.25 mm. Similar uncertainty would also be expected to exist between the temperature and concentration profiles.

Results and Discussion

To demonstrate the improvements provided by the split introduction of O_2 on the yields of C_{2+} products, two sets of experiments were performed. First, a single-bed experiment (SB1) was performed in which methane and oxygen were fed at a CH_4/O_2 ratio of 4.0 at 120 mL min^{-1} ($\approx$60 ms space time). In the first dual-bed experiment (DB1), the first reactor feed was at 120 mL min^{-1} having a CH_4/O_2 ratio of 9.0, followed by 12 mL min^{-1} O_2 addition into the interstage zone, which thereby maintained the overall CH_4/O_2 ratio of 4.0.

An additional dual-bed experiment was also performed at the overall CH_4/O_2 ratio of 4.4 (DB2 experiment) to assess the impact of the CH_4/O_2 ratio on reactor performance. In this case, the feed flow rate to the first reactor feed was kept at 120 mL min^{-1} with a CH_4/O_2 ratio of 11.0, followed by the introduction of 15 mL min^{-1} O_2 to the interstage zone. Notably, in the dual-bed experiments (DB1, DB2) both of the catalyst beds were kept inside one tubular furnace (Figure 1).

In Figure 2, the spatially resolved temperature and species mole percent profiles are presented for the single-bed reactor experiments (SB1). In Figures 3 and 4, the same profiles are presented for the dual-bed reactor experiments DB1 and DB2, respectively. A total of nine species were quantified: CH_4, O_2, C_2H_6, C_2H_4, C_3H_8/C_3H_6 (C_3), H_2, H_2O, CO, and CO_2. With the exception of H_2O concentration, which was calculated from oxygen atom balances, all the species were quantified directly from GC measurements by using multipoint GC calibration process performed before the OCM experiments. In Figure 5, the CH_4 conversion and C_{2+} ($C_2H_6+C_2H_4+C_3$) selectivity profiles are presented for the SB1, DB1, and DB2 experiments. Methane conversions and C_{2+} selectivities were determined from Equations (1) and (2):

$$CH_4 \text{ conversion } [\%] = \frac{[(CH_4)_{in} - (CH_4)_{out}]}{[(CH_4)_{in}]} \times 100 \quad (1)$$

$$C_{2+} \text{ selectivity } [\%] = \frac{[2\,(C_2H_6 + C_2H_4) + 3\,(C_3H_6)]}{[2\,(C_2H_6 + C_2H_4) + 3\,(C_3H_6) + CO_2 + CO]} \times 100 \quad (2)$$

In all the figures, the locations of the various sections of the reactor system are indicated by vertical dashed lines; the first La_2O_3–CeO_2 nanofiber fabric catalyst packing starts at approximately 5 mm and ends at approximately 15 mm, which corresponds to a bed depth of approximately 10 mm. The first 5 mm in the graphs correspond to the quartz-wool packing. The first bed is followed by another 5 mm of quartz packing, followed by 15 mm of interspace (no packing). The quartz packing for the second bed starts at approximately 35 mm followed by approximately another 10 mm La_2O_3–CeO_2 nanofiber

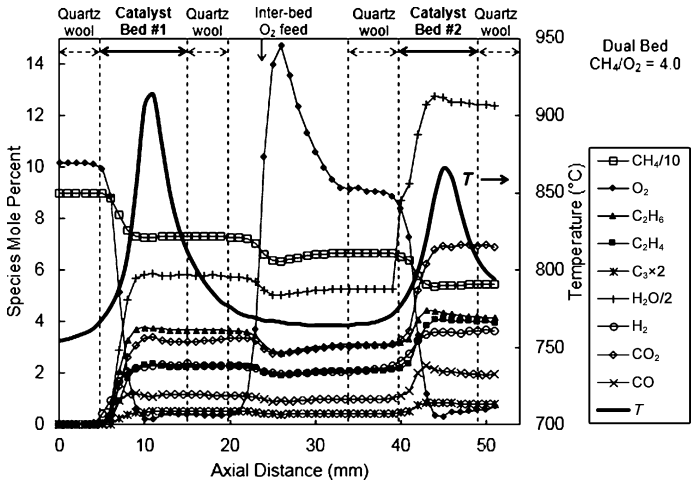

Figure 3. Spatial temperature and species mole percent profiles for the dual-bed reactor system (DB1). Feed to first reactor was 120 cm^3 s^{-1} STP at $CH_4/O_2 = 9$. Interbed O_2 flow rate was 12 cm^3 s^{-1} STP, which rendered overall $CH_4/O_2 = 4.0$.

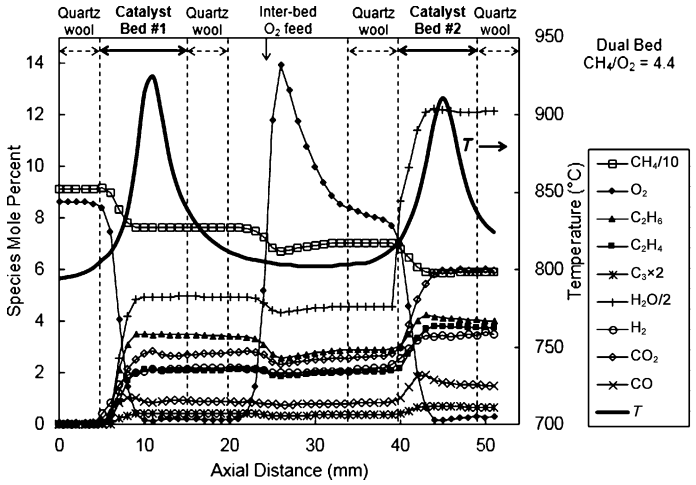

Figure 4. Spatial temperature and species mole percent profiles for the dual-bed reactor system (DB2). Feed to first reactor was 120 cm^3 s^{-1} STP at a $CH_4/O_2 = 11$. Interbed O_2 flow rate was 15 cm^3 s^{-1} STP, which rendered overall $CH_4/O_2 = 4.4$.

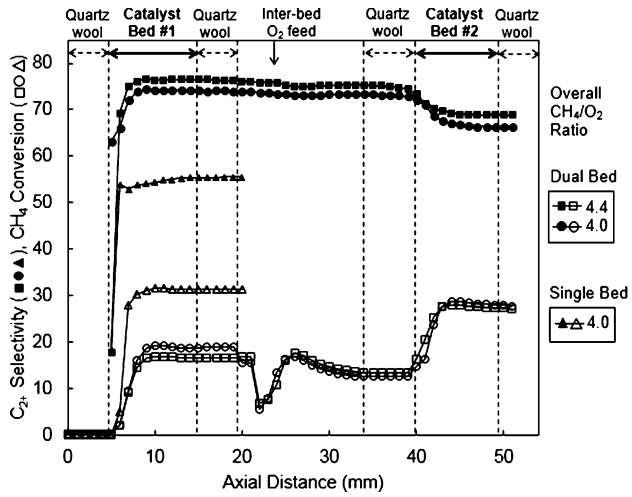

Figure 5. Spatial profiles for CH_4 conversions and C_{2+} selectivities for the single-bed (SB1) and dual-bed (DB1, DB2) experiments.

fabric catalyst and 5 mm of quartz-wool packing. The secondary O_2 injection point was at approximately 25 mm, as indicated by an arrow pointing down. Other than the interspace concentration profiles, the location of the O_2 injection point had no discernible effect on the performance of the second reactor.

The spatial concentration and temperature profiles for the single-bed experiment (SB1) with a CH_4/O_2 ratio of 4 were acquired at a furnace temperature (T_f) of 600 °C, which was sufficient to achieve ignition. As seen in Figure 2, the maximum bed temperature reached approximately 1015 °C at approximately 10 mm (i.e., 5 mm within the catalyst zone), concomitant with the near-complete consumption of O_2 and approximately 30% CH_4 maximum conversion and 55% C_{2+} selectivity (see also Figure 5). These values represent a C_{2+} yield of approximately 16%.

Close examination of the profiles at the upstream part of the catalyst bed reveals significant levels of H_2 production early in the catalytic zone, that is, prompt H_2; a peak level is reached at approximately 3.7 mol% within 3 mm inside the catalyst bed (8 mm axial distance). Within this zone, the reactor temperature is still relatively low at 650–725 °C; thus, H_2 formation is expected to be due to surface-catalyzed reactions. Hydrogen formation precedes H_2O formation (peak 19%) and is closely followed up by CO_2 (9.31%) and CO (≈3%) and then by C_2H_6 (3.6%).

The measured concentration profiles for C_2H_6 and H_2O are consistent with the well-established elementary reactions leading to their formation. Surface oxygen species [O] are widely accepted to be responsible for CH_4 activation leading to the formation of CH_3 radicals and surface [OH].[14–16] The CH_3 radicals then diffuse away from the catalyst surface and recombine in the gas phase to produce C_2H_6. Regeneration of the active sites is also well accepted to occur through the formation and desorption of H_2O.[14,15] The vacated active sites are then rapidly repopulated by O_2 chemisorption. These events are summarized by the following elementary reaction set [Eqs. (3)–(6)]

$$O_2 + 2[*] \rightarrow 2\,[O] \quad (3)$$

$$CH_4 + [O] \rightarrow CH_3 + [OH] \quad (4)$$

$$CH_3 + CH_3 \rightarrow C_2H_6 \quad (5)$$

$$[OH] + [OH] \rightarrow [O] + [*] + H_2O \quad (6)$$

in which [*] represents a vacant catalytic surface site for oxygen chemisorption. It is known that a dynamic equilibrium exists between gaseous O_2 and the various forms of surface oxygen, for example, chemisorbed and lattice oxygen. The early formation of H_2, which is also accompanied by H_2O, CO_2, and CO, could be attributed to surface reactions similar to those reported in the catalytic partial oxidation (CPO) of methane to synthesis gas on Pt and Rh surfaces,[17,18] or by reactions such as the following [Eqs. (7)–(13)]:

$$CH_3 + [OH] \rightarrow [CH_2O] + H_2 \quad (7)$$

$$[CH_2O] \rightarrow [*] + CO + H_2 \quad (8)$$

$$CO + [O] \rightarrow CO_2 + [*] \quad (9)$$

$$CH_3 + [O] \rightarrow [CH_3O] \rightarrow [CHO] + H_2 \quad (10)$$

$$[CHO] + [O] \rightarrow [*] + [H] + CO_2 \quad (11)$$

$$[CHO] \rightarrow [H] + CO \quad (12)$$

$$[H] + [H] \rightarrow 2\,[*] + H_2 \quad (13)$$

Undesired gas-phase reactions of CH_3 with O_2, O, and OH can also lead to CO_2 and CO (CO_x) formation, but at higher temperatures. Ethylene is then produced by the oxidative or catalytic dehydrogenation of C_2H_6. As a consequence, C_2H_4 formation exhibits significant lag relative to C_2H_6 formation, which is clearly observed in Figure 2. Ethylene levels peaked at 3.1% at 4 mm into the catalyst bed. Once formed, both C_2H_6 and C_2H_4 can also interact with [O] and result in the formation of CO_x as a result of both gas-phase and surface reactions.[14,15] Figure 2 also shows the early formation and rapid rise of H_2O concomitant with a decrease in the O_2 concentration. It is well recognized that the steady-state rate of the OCM reaction is controlled not by the activation of CH_4 and C_2H_6 formation, but by the reactions that lead to the formation of H_2O [e.g., Eq. (6)]. This is because of the requirement to close the catalytic cycle.[14,15] The data presented in Figure 2 are in harmony with this argument, for which sharp changes in species mole fraction profiles cease only after O_2 is completely consumed and H_2O formation level off.

The spatial concentration and temperature profiles for the dual-bed operation (DB1) for the OCM reaction at the overall CH_4/O_2 ratio of 4 as presented in Figure 3 reveal several important features. First, the feed CH_4/O_2 ratio of 9 used in the first catalyst bed necessitated the use of a higher T_f of approximately 750 °C for ignition. As seen in Figure 3, the bed temperatures rapidly increased within the catalytic zones and reached maximum bed temperatures of 920 °C in the first bed and 866 °C in the second bed, both at approximately 5 mm within the catalyst zones, which corresponds to complete conversion of O_2. This trend of temperature profile is similar to the SB1 experiment presented in Figure 2 and yet gives us additional insight into the effects of temperature on C_{2+} yields in OCM. For example, the peak temperatures in each bed for the dual-bed experiments are significantly lower than those in the single-bed experiment. This was the consequence of the split introduction of oxygen and heat removal realized within the interstage zone, which collectively decreased the maximum temperature attained in the OCM reactors, in spite of the higher ignition temperature. As seen in Figure 5, a C_{2+} selectivity of 70% and an ultimate C_{2+} yield of 21% was achieved in the DB1 experiment; the latter is a value significantly higher than the 16% yield observed in the single-bed experiment at the same overall CH_4/O_2 ratio of 4. This clearly demonstrates that distributing the oxygen feed with interstage cooling is a good strategy to increase CH_4 conversion, whereas adverse effects on the selectivity of C_{2+} products are minimized. These comparative results are also presented in Table 1.

Table 1. Reaction conditions and reactor exit values for conversions, selectivities, and yields.[a]

	T_f [°C]	Overall CH_4/O_2 ratio	T_{peak} [°C]	Feed 1 CH_4/O_2 ratio	Exit 1 CH_4 conv. [%]	Exit 1 C_{2+} sel. [%]	Exit 1 C_{2+} yield [%]	$T_{interbed}$ [°C]	$T_{peak\,2}$ [°C]	Exit 2 CH_4 conv. [%]	Exit 2 C_{2+} sel. [%]	Exit 2 C_{2+} yield [%]
SB1	600	4	1015	4	30	55	16	–	–	–	–	–
DB1	750	4	920	9	17	77	13	755	866	30	70	21
DB2	780	4.4	930	11	19	74	14	800	910	28	67	19

[a] 1 and 2 refer to catalyst beds.

Second, although the mixing of the secondary O_2 feed with the reactor gases was not instantaneous, as evidenced by the presence of a steep axial oxygen concentration profile, a uniform composition was achieved within the interbed zone close to the upstream quartz-wool packing of the second reactor. Third, the concentrations of all the species decreased upon O_2 introduction (i.e., dilution), but remained virtually unchanged along the interbed zone and within the quartz-wool packing. Furthermore, the temperature in the interbed zone remained at approximately 755 °C, close to the furnace temperature. These measurements clearly indicate both the absence of any gas-phase reactions and the inert nature of the quartz wool. This is a surprising result, as packets of high O_2 concentrations would be expected to cause gas-phase combustion at the indicated interbed temperatures especially if H_2 is present. The OCM reaction commenced once the gases entered the second catalytic bed at approximately 40 mm.

As seen in Figure 3, CO exhibited peak concentrations of 1.2% at 9 mm in the first bed and of 2.2% at 43 mm in the second bed, which ultimately leveled off at 2.0% at the reactor exit. Hydrogen levels were 2.3 and 3.6% at the exits of beds 1 and 2, respectively. Carbon dioxide and water levels reached 3.4 and 11.5% in bed 1, respectively, and became 7 and 25.5% at the exit of the dual-bed reactor, respectively.

Hydrocarbon products generally increased monotonically within the catalytic zones with increasing methane conversions and ceased to change if O_2 was consumed. At the exit of the first bed, the following levels were reached: C_2H_6 3.7%, C_2H_4 2.23%, and C_3H_6 0.25%, whereas CH_4 conversion was 17%. Under these conditions, C_{2+} selectivities corresponded to 76.6%, which represents a yield of 13%. However, at the exit of the second bed the species concentrations became: C_2H_6 4.4%, C_2H_4 4.1%, and C_3H_6 0.41%, whereas CH_4 conversion increased to approximately 30%, with a small reduction in the C_{2+} selectivities and, hence, a 21% yield at the end of the dual-bed reactor.

Temperature and species concentration profiles within the second catalytic zone were qualitatively similar to those within the first bed, and the reactions ceased immediately after the exhaustion of O_2. This is an interesting result because unlike the first reactor, the feed to the second catalyst bed possessed significant levels of H_2, CO, CO_2, and H_2O, together with C_{2+} products. Considering the fact that with complete consumption of oxygen in the second bed, H_2 and H_2O production levels are consistent with our expectations from the OCM reaction and there is no sign of H_2O consumption in the second bed. Therefore, as apparent from the species concentration profiles in the second bed, even in the presence of an excess amount of steam produced in the first bed, La_2O_3–CeO_2 does not promote the steam reforming of methane reaction. Moreover, the excess amounts of carbon dioxide and water fed to the second bed did not cause any apparent deactivation of the OCM catalyst.

Analysis of the experimental data of Figures 2 and 3 also indicate that the catalytic water gas shift (WGS) reaction, that is, $H_2O + CO \rightleftharpoons CO_2 + H_2$, can be ruled out. For example, the mole fraction ratios $Y_{CO_2} x Y_{H_2}/(Y_{H_2O} x Y_{CO})$ were in the 0.4–0.6 range within the 5 mm in the catalyst beds in all the experiments. These values are significantly lower than those of the WGS reaction equilibrium constants that are in the 1.5–2.0 range under the prevailing conditions in the reactor beds.

The profiles for the DB2 experiment at the overall CH_4/O_2 ratio of 4.4 as presented in Figure 4 are in harmony with the DB1 experiment at $CH_4/O_2 = 4.0$ (Figure 3), which thereby gives us confidence regarding the validity of our measurements. In the DB2 experiment, the feed CH_4/O_2 ratio of 11 used in the first catalyst bed necessitated the use of a higher T_f of approximately 780 °C for ignition, and the maximum bed temperatures reached 930 and 910 °C in the first and second beds, respectively. These values are significantly lower than the single-bed temperature peak of 1015 °C (Figure 2). Again, the location of the maximum temperatures corresponds to the complete conversion of O_2. Moreover, the interbed temperature remained relatively constant at approximately 800 °C.

From Figure 4 it can be seen that CO exhibited a peak concentration of 1.0% at 5 mm within the first bed, and ultimately reached 1.6% at the exit of the second catalyst bed. Hydrogen levels were 2.2 and 3.5% at the exits of beds 1 and 2, respectively. Carbon dioxide and water levels reached 2.8 and 10% in bed 1, respectively, and became 6 and 24.2% at the exit of the second bed, respectively.

In the DB2 experiment, the hydrocarbon products also exhibited similar trends, which generally increased within the catalytic zones with increasing methane and oxygen conversions and which ceased to change after the complete conversion of O_2. At the exit of the first bed, the following levels were recorded: C_2H_6 3.52%, C_2H_4 2.1%, and C_3H_6 0.21%, whereas CH_4 conversion was 19%. Under these conditions, C_{2+} selectivities would be 74%, which represents a yield of 14%. At the second bed exit, the concentration levels became C_2H_6 4.1%, C_2H_4 3.8%, and C_3H_6 0.35%, with a maximum CH_4 conversion of approximately 28%. These results correspond to a C_{2+} selectivity of 67% and represent a final yield of approximately 19%. This value is slightly lower than the 21% yield obtained in the DB1 experiment yet higher than the 16% yield of the single-bed experiment (see Table 1).

Conclusions

The microprobe sampling technique as applied to dual-packed-bed catalytic reactors for the oxidative coupling of methane (OCM) demonstrated that distributing the O_2 feed can significantly increase the yields of the C_{2+} products. By using La_2O_3–CeO_2 nanofiber fabric catalyst beds, the C_{2+} products were obtained in an ultimate yield of 21% in a double-bed OCM reactor with split O_2 introduction, which is significantly higher than the 16% yield observed in the single-bed experiment at the same overall CH_4/O_2 ratio of 4. The dual-bed configuration with interstage cooling increases the yield of the C_{2+} products primarily by increasing CH_4 conversion and by maintaining the C_{2+} product selectivity levels.

Acknowledgements

We thank LCS for the use of their facilities and database. B.Z. acknowledges the National Science Foundation (NSF) GRFP Support Grant No. DGE1144087 and the University of California, Los Angeles (UCLA) Graduate Division Fellowship. D.N. acknowledges NSF MCTP–DGE-0654431 Fellowship.

Keywords: gas-phase reactions · microreactors · nanostructures · oxidation · surface chemistry

[1] M. C. Alvarez-Galvan, N. Mota, M. Ojeda, S. Rojas, R. M. Navarro, J. L. G. Fierro, *Catal. Today* **2011**, *171*, 15 – 23.
[2] U. Zavyalova, M. Holena, R. Schlögl, M. Baerns, *ChemCatChem* **2011**, *3*, 1935 – 1947.
[3] S. Sahebdelfar, M. T. Ravanchi, M. Gharibi, M. Hamidzadeh, *J. Nat. Gas Chem.* **2012**, *21*, 308 – 313.
[4] C. Hammond, S. Conrad, I. Hermans, *ChemSusChem* **2012**, *5*, 1668 – 1686.
[5] E. Esche, H. Arellano-Garcia, L. T. Biegler, *AIChE J.* **2014**, *60*, 170 – 180.
[6] S. Jašo, H. R. Godini, H. Arellano-Garcia, M. Omidkhah, G. Wozny, *Chem. Eng. Sci.* **2010**, *65*, 6341 – 6352.
[7] E. V. Kondratenko, U. Rodemerck, *ChemCatChem* **2013**, *5*, 697 – 700.
[8] B. Zohour, D. Noon, S. Senkan, *ChemCatChem* **2013**, *5*, 2809 – 2812.
[9] a) J. W. Thybaut, J. Sun, L. Olivier, A. C. Van Veen, C. Mirodatos, G. B. Marina, *Catal. Today* **2011**, *159*, 29 – 36; b) J. Sun, J. W. Thybaut, G. B. Marin, *Catal. Today* **2008**, *137*, 90 – 102.
[10] J. H. J. B. Hoebink, P. M. Couwenberg, G. B. Marin, *Chem. Eng. Sci.* **1994**, *49*, 5453 – 5463.
[11] D. Noon, A. Seubsai, S. Senkan, *ChemCatChem* **2013**, *5*, 146 – 149.
[12] R. Horn, O. Korup, M. Geske, U. Zavyalova, I. Oprea, R. Schlögl, *Rev. Sci. Instrum.* **2010**, *81*, 064102-1-6.
[13] O. Korup, S. Maylyankariev, M. Geske, C. F. Goldsmith, R. Horn, *Chem. Eng. Process.* **2011**, *50*, 998 – 1009.
[14] M. Y. Sinev, Z. T. Fattakhova, V. I. Lomonosov, Y. A. Gordienko, *J. Nat. Gas Chem.* **2009**, *18*, 273 – 287.
[15] Z. Stansch, L. Mleczko, M. Baerns, *Ind. Eng. Chem. Res.* **1997**, *36*, 2568.
[16] S. Senkan, *Advances in Chemical Engineering: 18*, Academic Press, New York, **1992**, 95.
[17] D. A. Hickman, L. D. Schmidt, *Science* **1993**, *259*, 343 – 346.
[18] D. Dalle Nogare, N. J. Degenstein, R. Horn, P. Canu, L. D. Schmidt, *J. Catal.* **2011**, *277*, 134 – 148.

Received: June 3, 2014
Published online on August 27, 2014